ACS APPLIED NANO MATERIALS

www.acsanm.org Article

Self-Assembled Arrays of Gold Nanorod-Decorated Dielectric Microspheres with a Magnetic Dipole Response in the Visible Range for Perfect Lensing and Cloaking Applications

Rossella Grillo,* Dominik Beutel, Ugo Cataldi, Carsten Rockstuhl, and Thomas Bürgi*

Cite This: *ACS Appl. Nano Mater.* 2020, 3, 6108−6117 Read Online

ACCESS | Metrics & More | Article Recommendations

ABSTRACT: Photonic nanostructures made of a dielectric sphere covered with many metallic nanospheres fabricated by self-assembly constitute a basic building block for optical metamaterials with a magnetic response in the visible. However, they suffer from limited degrees of freedom to tune their response. Once the involved materials are chosen, the response is mostly determined. To overcome such a limitation, we design, fabricate, and characterize here a bottom-up metamaterial in which metallic nanorods are used instead of nanospheres. Nanorods offer the ability to tune the spectral position of the resonances by changing their aspect ratio. Building blocks consisting of dielectric spheres covered with metallic nanorods are fabricated and characterized. They are also deposited in densely packed arrays on a substrate using a blade coating deposition of the dielectric spheres first and a subsequent deposition of the metallic nanorods. Full-wave optical simulations support the spectroscopic characterization. These simulations also indicate a dominant magnetic dipolar response of the building blocks. These arranged core−shell structures are promising materials for applications such as perfect lensing and cloaking.

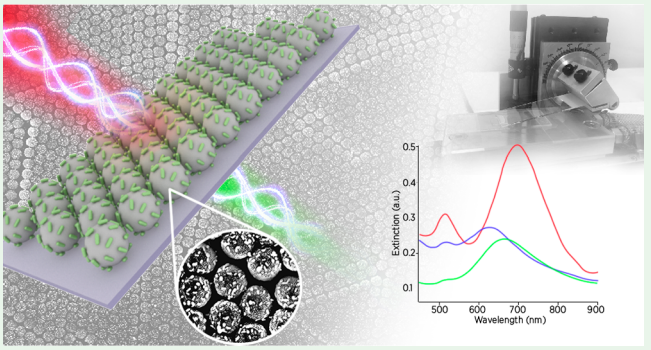

KEYWORDS: *metamaterials, core−shell nanostructures, isotropic magnetic resonance, gold nanorods, bottom-up techniques, self-assembly, colloidal nanochemistry*

INTRODUCTION

The ability to arrange many metallic nanoparticles on the surface of a dielectric sphere, an arrangement that we will call here a core−shell cluster, attracted quite some interest from the metamaterial community.[1−4] The interest arose because it is an elementary building block with a strong magnetic response at optical frequencies.[5−7]

The rationale behind the design relies on the fact that the metallic nanoparticle sustains at a selected wavelength a localized surface plasmon polariton (LSPP). For a sufficiently small spherical nanoparticle, the LSPP is excited at the wavelength at which the permittivity of the metal is negative and in magnitude twice the permittivity of the surrounding medium. For noble metals such as gold or silver, this condition is met in the visible. By arranging many metallic nanospheres on top of a larger dielectric sphere that is, nevertheless, small compared to the relevant wavelength, a ring type current is induced that gives rise to a strong magnetic dipole moment for the entire building block.[8] The magnetic dipole is driven into resonance at longer wavelengths when compared to the localized surface plasmon resonance (LSPR) of the isolated nanosphere thanks to their mutual coupling. Packing such building blocks in a dense manner is the key to achieve metamaterials with tailored optical properties on demand.[5,9,10] A magnetic response at visible wavelengths,[11] for example, is a crucial requirement for many fascinating applications, such as perfect lensing[12] or cloaking.[13]

Due to their geometry and the small size relative to the wavelengths of incident radiation, core−shell clusters are isotropic, which is a clear advantage when compared to many other building blocks suggested for similar purposes. Indeed, many other structures, such as the split-ring resonator,[14] exhibit a high level of anisotropy.[15] They sustain a magnetic response only upon illumination along one specific crystallographic axis while for other directions no magnetic response can be observed. The core−shell clusters share that benefit of an isotropic response with alternative approaches that rely on spherical beads.[16] Indeed, spherical beads made from either

Received: May 17, 2020
Accepted: May 21, 2020
Published: May 21, 2020

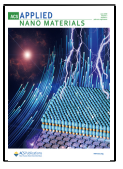

https://dx.doi.org/10.1021/acsanm.0c01346
ACS Appl. Nano Mater. 2020, 3, 6108−6117

polaritonic materials[17] or high-index dielectric materials such as silicon can be tailored to support a strong magnetic dipolar response.[18−20] While for polaritonic materials the operational wavelength is fixed, for spheres made from high-index dielectric materials changing the size allows tuning of the resonance wavelength. Also, structures such as the core−shell clusters or the high-index dielectric spheres can be fabricated with bottom-up technologies in rather large quantities on reasonable time scales. Using top-down nanostructuring technology makes it complicated to achieve bulk materials, and mostly thin films are realized only. This led to the notion of metasurfaces rather than metamaterials. Combining top-down and bottom-up might solve the problem of the anisotropy, but still, the desire to have bulk materials at hand strongly favors bottom-up self-assembly methods.[21]

However, the existing approach where metallic nanospheres decorate the core dielectric sphere has some limitations. In particular, because the resonance wavelength of the nanosphere is basically fixed once the material from which it is made has been chosen, there is nearly no degree of freedom left to tune the resonance wavelength of the induced magnetic dipole moment. Changing the density of the nanospheres to suppress their mutual coupling and to tune in that way the resonance wavelength is not really an option. It compromises the oscillator strength and with that the possible dispersion in the material properties. Also, changing the size of the core sphere does not really help to tune the resonance wavelength, as only a narrow size window exists where the dipole moments of the response dominate. Of course, it has been demonstrated that making the core sphere larger can shift the resonance wavelength,[22] but we quickly enter a regime where many multipole moments are supported and then a homogenization and a description with, ideally, local constitutive relations is not possible anymore.

To overcome such limitation we suggest in this contribution to use gold nanorods (GNRs) instead of nanospheres. Changing the aspect ratio of the nanorods allows a continuous tuning of their LSPR wavelength. This translates to a tunable resonance wavelength for the entire building block that consists of assembled GNRs on the surface of the dielectric core sphere.

In our work we design, fabricate, and characterize such building blocks, which are attractive for applications such as perfect lensing or cloaking.[12,23] We explore the subtle interplay between the mutual coupling of the GNRs on top of the core dielectric sphere and the dielectric environment that leads to a spectral shift of the resonances. To elucidate these effects, we systematically study the pertinent material with increasing complexity. We start from the isolated GNRs in solution and continue to study GNRs deposited on planar glass substrates and on silica spheres. The latter are either in solution or deposited as dense films on a glass substrate. This work combines preparative work, including surface chemistry and self-assembly, with microscopic and optical characterization. The measured scattering responses are compared to full-wave optical simulations. These simulations are based on the T-matrix method.[24] There, the scattering response of an individual particle can be obtained analytically or numerically based on its shape and material properties. It is encoded in a matrix, the so-called T-matrix. The coupling of the particles, namely the GNRs and dielectric spheres, taking into account all multiple-scattering processes that occur, can be calculated analytically, using the T-matrices and the relative positions.

RESULTS AND DISCUSSION

General Assembly Procedure. Optimized GNRs with respect to size and aspect ratio are self-assembled in the following onto dielectric spheres using chemical functionalization approaches that exploit electrostatic interactions. A variety of driving forces can induce the spherical assembly of metallic nanoparticles of different sizes and shapes.[4,25−27] Electrostatic self-assembly has proven to be a flexible method that can be easily applied for obtaining robust core−shell clusters in high yield.[4,8,28] Subsequent to the preparation of different building blocks in solution and to the measurement of their scattering response, the next step involves their organization on surfaces.

We designed and built a dedicated laboratory apparatus (see Figure 1) to perform blade coating of colloidal samples under

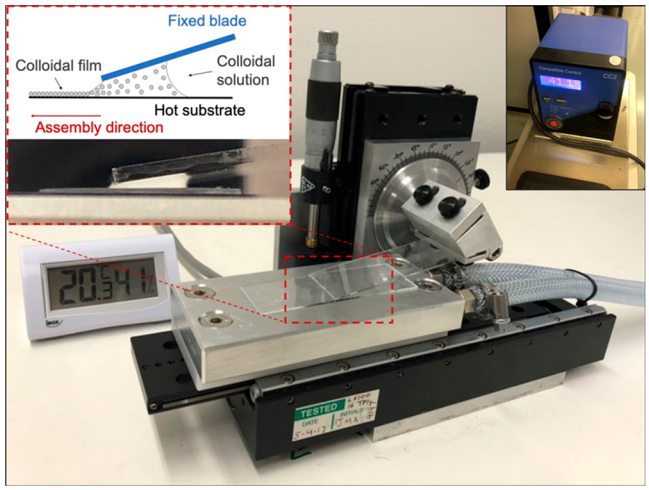

Figure 1. Home-built blade coating apparatus. A schematic illustration of the colloidal assembly and a magnification of the corner between the blade and the substrate is shown in the red dashed inset. The system is placed inside a plexiglass box and connected to a laboratory thermostat, shown in the top right corner. A hygrometer is installed to monitor the ambient humidity.

well-controlled conditions. Using this apparatus, we fabricated large area monolayers of perfectly ordered silica microspheres. Glass microscope slides were employed as both substrates and blades. The blade coating system consists in a translation stage that moves at very low speeds (below micrometer/sec). An aluminum plate is positioned on top of the translation stage and connected to a laboratory thermostat (see the inset in Figure 1). The substrate is fixed on this plate that, due to the high thermal conductivity of aluminum, keeps its temperature constant for the duration of the deposition. A blade is placed and fixed at an adjustable angle immediately above the substrate. A small opening enables injection of the sample. Finally, the velocity of the substrate, that is, the motional speed of the translation stage, is set through a dedicated software. Such a configuration allows the preparation of sample areas up to a few square centimeters in size within the time scale ranging from a few minutes to a couple of hours at maximum.

Blade coating deposition ensures several advantages over other coating techniques. Very homogeneous films and patterns can be deposited on multiple square centimeters on a time scale that goes from a few minutes to a couple of hours. Moreover, this technique offers precise control and reduced material consumption in contrast to dip coating and spin coating. It is a relatively parsimonious method, and with some

https://dx.doi.org/10.1021/acsanm.0c01346
ACS Appl. Nano Mater. 2020, 3, 6108−6117

practice the loss of coating solution can be minimized. This aspect should not be underestimated because it permits the deposition of well-designed films when very little (precious) material is available. Furthermore, the film thickness can also be adjusted and the technique yields reproducible results. The assembly mechanism that drives blade coating deposition of close-packed monolayers is convective assembly.[29] This mechanism is based on the confinement of particles induced at the three-phase contact line of a colloidal solution that is dragged over a substrate, and it depends on the wetting properties of the substrate. Convective assembly occurs on hydrophilic substrates and arises from the convective flow of the solution induced by evaporation at the contact line of the droplet, which, on flat substrates, determines the creation of close-packed films. This method allows obtaining a perfectly ordered close-packed array of core−shell clusters. Please note, in our work we first deposit the dielectric core spheres on the glass substrate and deposit afterward the GNRs on top of them using a dip coating technique.

Gold Nanorods. The method adopted for the GNRs synthesis was the so-called seed-mediated growth method.[30] This approach disconnects the nucleation and growth steps to avoid the creation of unwanted particles with other shapes. Basically, the synthesis method comprises the preparation of very small (4−5 nm in diameter) spherical gold nanoparticles (seeds), which are successively added to the growth solution in a micellar environment for the GNRs development.

Is well-known that the longitudinal band of GNRs can be tuned by changing their aspect ratio (AR).[31] With the seed-mediated growth method, it was possible to control the length of the GNRs by changing the silver ion content in the growth solution. It was found that by increasing the silver ion content, the AR of the rod increases, resulting in a gradual red-shift and broadening of the longitudinal plasmon band. From back-of-the-envelope considerations, where the resonance wavelength of the GNR is related to the AR,[32] it can be estimated that the AR changes from 2.4 to 3.98 for the different samples, supported by data obtained from transmission electron microscopy (TEM) images.

Figure 2 shows the UV−vis spectra of several GNRs solutions obtained by adding different volumes (from left to right: 0.31 mL, 0.4 mL, 0.5 mL, 0.63 mL, 0.75 mL, 0.88 mL) of silver nitrate (4 mM) while all the other reagents in the growth solution remain unchanged (for synthesis details, see the dedicated section). In such a manner, the longitudinal plasmon band could be tuned across a wide spectral region from 653 to 800 nm.

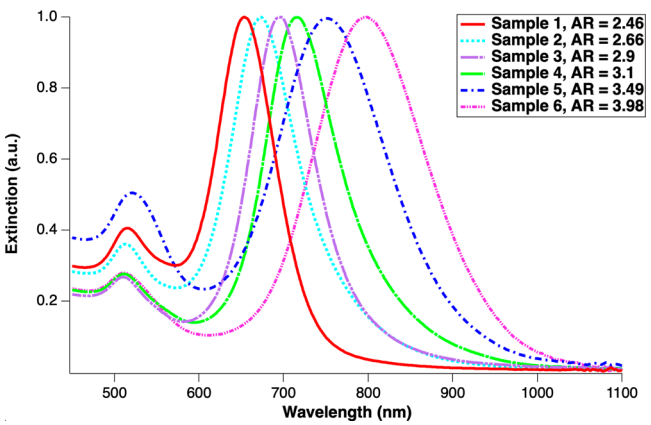

Figure 2. UV−vis spectra of several solutions of gold nanorods with different aspect ratios.

The TEM images of five of the six samples of GNRs related to the UV−vis spectra of Figure 2 are shown in Figure 3. Their

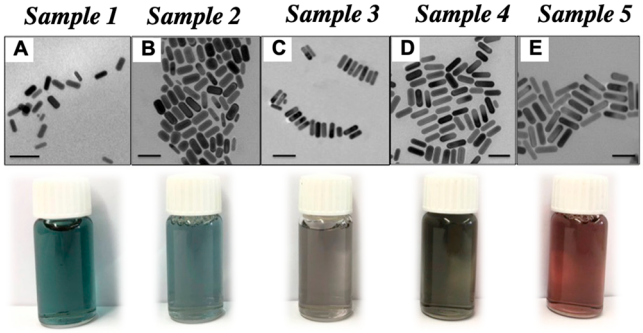

Figure 3. From A to E: TEM images of gold nanorods of increasing aspect ratio. Below each image are photographs of the corresponding solutions. Scale bar in TEM images: 50 nm.

different aspect ratios (increasing from left to right) translate to different colors of the corresponding solutions. This can be seen from the photographs that were taken from the actual solutions, as shown in the bottom of Figure 3.

After the synthesis, CTAB-stabilized GNRs were converted into citrate-stabilized GNRs by using the method of Mehtala et al.[33] with some modifications. The alteration of the surface chemistry of the GNRs was necessary to impart a negative charge, above all, and thus to create an electrostatic interaction with the functionalized silica microspheres. Moreover, CTAB-coated GNR dispersions are frequently not stable due to the ability to exchange and remove the surfactant.[33] For the same reason, residuals of CTAB can produce surface charge defects, without mentioning that CTAB is moderately cytotoxic.[34] The capping change of GNRs from CTAB to citrate was demonstrated by measuring the ζ-potential before and after the exchange process, which switched from a value of +15 mV to a value of −41.3 mV.

Core−Shell Clusters in Solution. The fabrication of the core−shell structures in solution was not straightforward. Extensive optimization was necessary in order to achieve a good surface coverage. The optimization included adjusting the ratio between GNRs and silica microspheres, changing the pH of the GNRs solution, choosing their optimal aspect ratio, and controlling the rate of stirring and the rate of addition of the silica microspheres into the GNRs solution. Finally, an optimal procedure was found as documented in the experimental section. GNRs obtained using 0.31 mL of silver nitrate were considered in the following experiments, corresponding to GNR with a main length of 38 nm and main diameter of 15 nm. Adding different amounts of silver nitrate allows acquisition of GNRs with different aspect ratios. However, synthesizing GNRs of a specific AR is quite challenging. The synthesis is very sensitive to various environmental parameters, such as the ambient temperature or the purity of the water or even the degree of cleanliness of the flasks used.[35] It often happens that the size distribution of the GNRs is not very sharp, which translates in a broad longitudinal resonance.

The arrangement of the GNRs into a spherical geometry results in changes of the optical properties with respect to

https://dx.doi.org/10.1021/acsanm.0c01346
ACS Appl. Nano Mater. 2020, 3, 6108−6117

GNRs considered individually, due to plasmonic coupling effect.[9] Figure 4 shows the measured extinction spectrum of

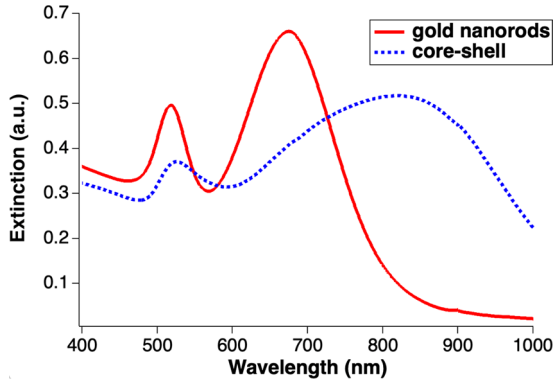

Figure 4. Comparison between the measured UV−vis spectra of the single gold nanorods (solid red line) and of the core- shell clusters (dashed blue line) in solution.

core−shell clusters composed of the GNRs and a 310 nm silica microspheres as the core sphere (blue trace) compared to the extinction spectrum of the GNRs in solution (red trace). A large red-shift (almost 200 nm) of the plasmonic resonance occurs when the GNRs are arranged into a spherical geometry. The measurements are done in the same solvent. Therefore, a modified dielectric environment cannot explain the shift in the resonance wavelength. Instead, this red-shift of the longitudinal plasmon band has to be explained by the coupling taking place in the spherical arrangement of all the nanorods and their rather high filling fraction on top of the spherical surface.[36]

Figure 5 presents a representative TEM image of the core−shell clusters. Silica microspheres appear fully covered by a large number of GNRs. On the grid, a notable quantity of free GNRs is not seen, except in close proximity to the microspheres. The absence of a large amount of free GNRs indicates that almost all GNRs cover the microspheres, meaning that a good ratio GNRs/SiO_2 microspheres was

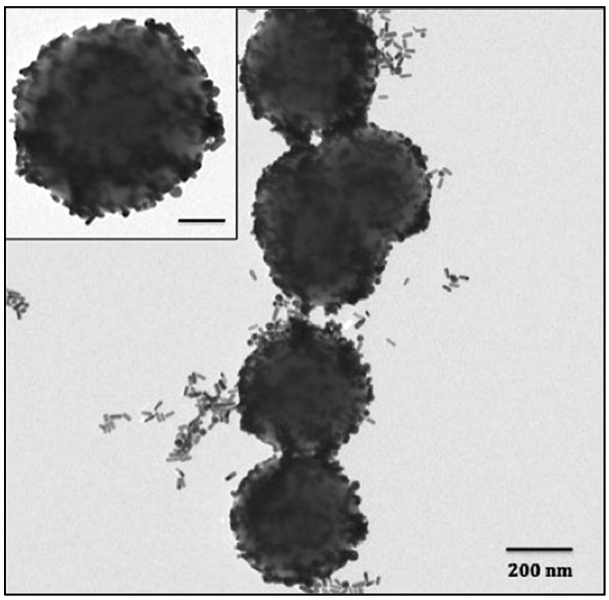

Figure 5. TEM image of core−shell cluster composed of 310 nm silica microsphere decorated with low aspect ratio gold nanorods.

chosen in the fabrication process of the core−shell clusters in solution. The assembly was therefore successful.

The fabrication of the core−shell structures described above is quite flexible. It is therefore possible to vary the materials and dimensions of both the dielectric core and surrounding particles, and therefore to fine-tune the optical properties of the composite materials.

Core−Shell Clusters Array. As shown in Scheme 1, a combination of blade coating and dip coating techniques

Scheme 1. Graphical Representation of the Experimental Procedure to Fabricate an Array of Core−Shell Nanoclusters

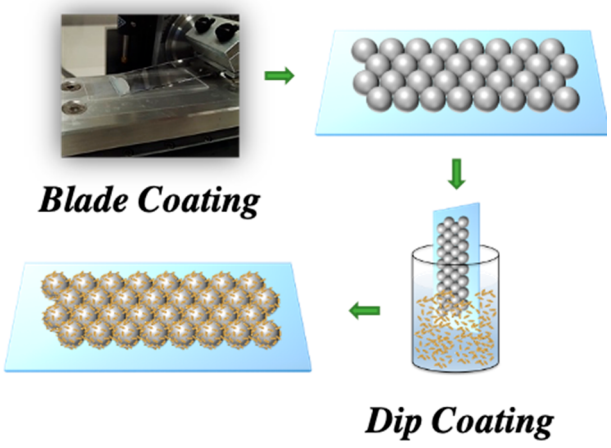

makes it possible to cover a monolayer of close-packed silica microspheres with GNRs, thus creating an array of core−shell nanoparticles.

Figure 6A shows the scanning electron microscopy (SEM) micrograph of a core−shell cluster array composed of silica microspheres coated by GNRs. In the inset of Figure 6A, a micrograph taken at higher magnification clearly shows the presence of GNRs on top of the silica microspheres. The silica monolayer appears homogeneously covered with a large number of nontouching GNRs. This uniform spherical arrangement of the GNRs determines the optical properties of such a structure.

The measured extinction spectrum of the core−shell cluster array composed of GNRs coated silica microspheres is displayed in Figure 7. The results are compared to the measured extinction spectra of individual GNRs (main AR of 2.9) dispersed in solution and deposited on a glass substrate. SEM micrographs of the GNRs deposited on a glass substrate are displayed in Figure 6B. The images show a dense array of randomly oriented GNRs. The plasmon resonances of the GNRs deposited on the glass substrate and on the silica microspheres monolayer, occurring respectively at 665 nm and at 627 nm, are strongly blue-shifted when compared to the resonance of the GNRs in solution, occurring at 696.5 nm. To explain this behavior, several factors have to be taken into account. All of them affect the spectral position of the resonance and shift them either to the blue or to the red.

First, there is a modified dielectric environment of the different samples. In general, a large refractive index in a surrounding medium shifts the resonance toward longer wavelengths. That likely explains a large fraction of the shifts observed in these figures as the GNRs in solution are

https://dx.doi.org/10.1021/acsanm.0c01346
ACS Appl. Nano Mater. 2020, 3, 6108−6117

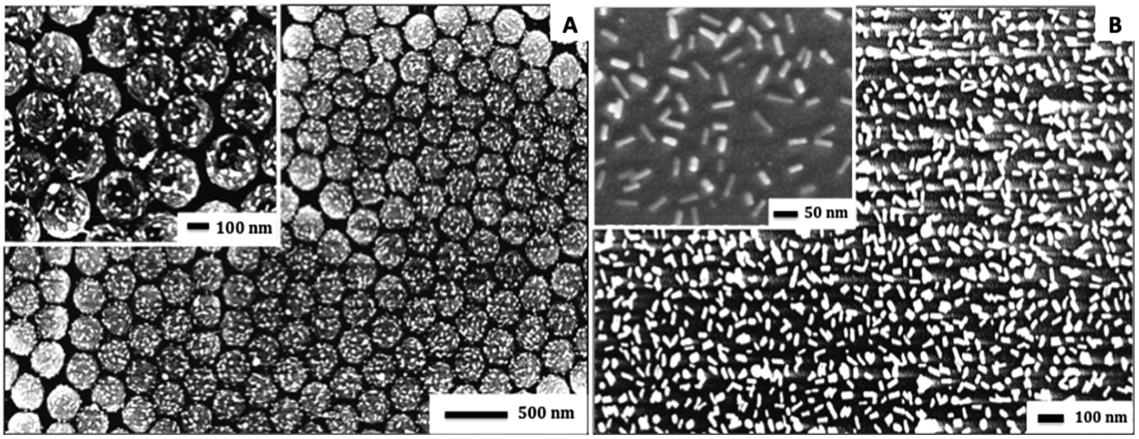

Figure 6. (A) SEM micrograph of a core−shell clusters array composed of silica microspheres decorated with gold nanorods. The inset shows a higher magnification micrograph where the presence of the nanorods on the silica surface is clearly visible. (B) SEM micrograph of gold nanorods deposited on a glass substrate. The higher magnification image displayed in the inset shows that the gold nanorods are randomly oriented.

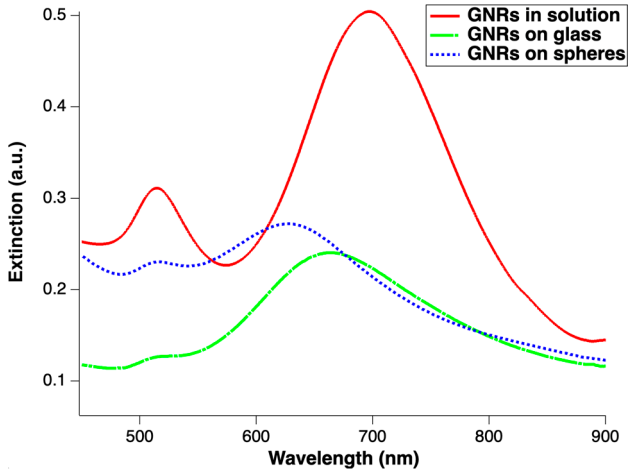

Figure 7. Comparison between the measured extinction spectra of the gold nanorod in solution (solid red line), deposited on glass substrate (dash-dotted green line), and deposited on the monolayer of silica microspheres (dotted blue line).

immersed entirely in a medium with a larger refractive index. In contrast, the GNRs on top of the glass substrate and on top of the silica microsphere are surrounded by air and only a fraction of the plasmonic fields exponentially confined to the GNRs will probe the presence of the high refractive index glass or silica environment. Thus, the shift toward longer wavelengths is likely less pronounced in the case of nanorods on a substrate or sphere compared to the complete embedding in the case of the nanorods in solution.

Second, it could be that in the deposition process a certain preference exists for only shorter GNRs to adhere to the glass or silica surfaces. The selective exclusion of large particles in dip-coated samples has been already observed.[37] This is also a plausible explanation considering the rather large line width of the sample with the GNRs in solution, indicating a polydisperse sample.

Third, coupling effects play a major role. We shall consider them separately for the sample where the GNRs are deposited on the glass substrate and on the silica microspheres.

Considering GNRs uniformly deposited on a glass substrate quite apart from each other would not lead to coupling effects, the LSPR position would not shift compared to that of the GNRs in solution except the shift that happens for the modified surrounding medium. However, as we can see in the SEM images in Figure 6B, the GNRs are rather densely packed, which leads to the appearance of coupling effects. Now, whether a red or a blue shift of the plasmon resonance happens depends on whether the nanorods are aligned side-to-side or end-to-end.[36] In general, all possible scenarios are encountered in our disordered sample, and the final direction of the shift based on such a coupling effect is hard to predict *a priori*. Similarly, for the GNRs deposited on the silica microspheres monolayer, the spectral position of the resonances changes because of the collective coupling effects of all the nanorods arranged on the spherical surface. That shift is usually toward a longer wavelength and is more pronounced for a larger surface filling fraction of the nanorods. However, just as for the discussion above on the coupling of the GNRs on the planar glass surface, the presence of nanorods at a short distance in a side-to-side or end-to-end configuration can shift the resonance toward shorter or longer wavelengths, respectively.

Fourth, for the GNRs deposited on the silica microspheres monolayer a final effect has to be considered. That is a coupling among the periodically arranged building blocks. The building blocks shall not be considered as isolated but rather densely packed and periodically arranged.

The precise disentanglement of all these effects is cumbersome. To verify in each case the final response, we resort here to full-wave optical simulations to understand major effects. Results are shown in Figure 8. Various systems are considered and compared qualitatively to the spectra shown in Figure 7.

First of all, we simulated isolated GNR in solutions (solid red line). The resonance at around 700 nm is well visible, corresponding to the measured resonance. Please note, the line width of the simulated extinction spectra is much narrower than the measured one because only a particle with a single dimension has been considered (see section on Characterization Techniques and Simulations). Dispersion in the size of the GNR changes their individual resonance wavelength, leading to an inhomogeneous broadening. The disordered arrangement in the solution has been, however, fully taken into account, as we considered the averaged response across all possible orientations. It remains to be mentioned that the resonance wavelength of the GNR in vacuum would be at

https://dx.doi.org/10.1021/acsanm.0c01346
ACS Appl. Nano Mater. 2020, 3, 6108−6117

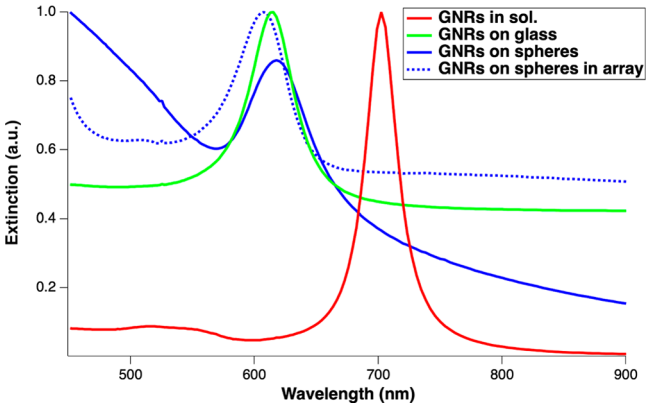

Figure 8. Simulated spectra of gold nanorods in solution (solid red line), on a glass substrate (solid green line), on the silica microspheres (solid blue line), and for the periodically arranged silica microspheres (dotted blue line). The extinction is scaled in all cases to a maximum value.

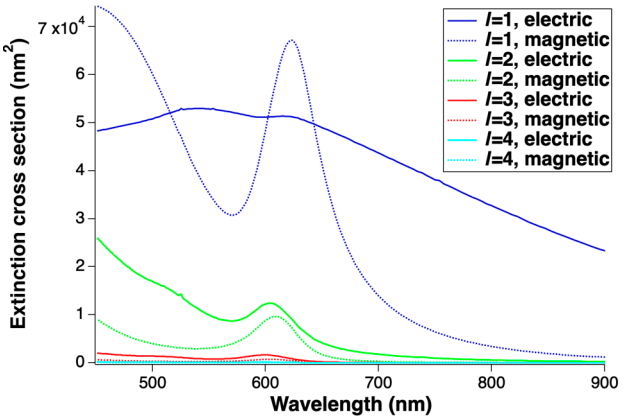

Figure 9. Contribution of the different multipole moments to the extinction spectra for an isolated silica microsphere decorated with gold nanorods.

approximately 580 nm (not shown). Therefore, the modified optical environment with a rather large index explains a notable fraction of the shift.

Next we look on the GNRs deposited on the glass substrate (solid green line). Following the procedure described in the section on Characterization Techniques and Simulations, we consider periodically arranged GNR leading to samples with the same surface filling fraction as experimentally encountered and average for a sample at normal incidence across all polarizations and across all possible orientations for the GNR in the unit cell. This leads to some unit cells with a pronounced side-to-side as well as end-to-end coupling. All coupling scenarios are considered with equal probability. The finally predicted resonance wavelength is in good agreement with the experiment. It appears blue-shifted when compared to the resonance wavelength of the GNRs in solution.

For the GNRs on the silica microsphere, we do see roughly the same resonance wavelength (solid blue line) as for the GNRs deposited on the glass substrate. In lowest order approximation, the resonance occurs in the same spectral region as for the sample where GNRs are deposited on the glass substrate, but in detail we notice that it is red-shifted, while in the experiments a blue-shift has been noticed. Therefore, a small effect must come from the interaction with the other silica microspheres that are periodically arranged. Only when this effect is considered (dashed blue line), is the correct order of the appearance of the resonance in the simulations just as observed in the experiment restored.

With the confidence that the experimental situation is well captured, we study the contribution of the different multipole moments to the extinction cross section. We consider an isolated silica microsphere decorated with GNRs. Results are shown in Figure 9 up to multipolar order $l = 4$. We distinguish the contribution of electric and magnetic multipole moments.[38] It can be seen that a nonzero contribution exists only up to the order $l = 3$, justifying our truncation of the multipolar order to $l = 4$. We do see a broadband response that comes from the electric dipolar order (solid blue curve). This has two local maxima (rather weakly pronounced though) around 520 and 600 nm. This is likely reminiscent to the response from the individual GNRs that have a pure electric dipolar response.

From the application perspective most important is the identification of the resonance at around 600 nm with a strong magnetic dipolar contribution (dashed blue line). The sample had been designed for such response and we clearly see that it acts as an artificial magnetic dipolar building block. There is a small contribution via the quadrupole moments but their response is rather weak.

The physical explanation for the appearance of that strong magnetic dipolar response is best illustrated in Figure 10. The

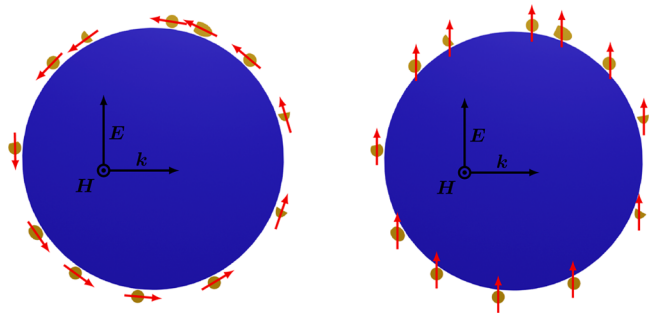

Figure 10. (Left) Conceptional picture to explain the strong magnetic dipolar resonance of the core−shell−particle. The small GNR on top of the dielectric core sphere sustains each an individual electric dipolar response that is driven into resonance once the localized plasmon polariton is excited. Due to their arrangement on the core sphere, a collective mode exists, as illustrated here, where all the dipoles are excited at a different phase, giving rise to the strong magnetic dipolar response at a resonance wavelength. (Right) The same configuration is shown but excited at a different wavelength, in which the electric dipoles in all the GNR are excited in phase, giving rise to a large electric dipole moment for the entire structure.

GNRs on top of the dielectric core sustain at a tunable wavelength a localized plasmon polariton. The larger the aspect ratio the stronger that resonance is tuned toward longer wavelengths. At this wavelength, the electric dipolar response of the individual GNR is driven into resonance. The random orientation of the GNR changes neither the resonance wavelength nor the multipolar character of the response of the individual GNR but only the magnitude with which each GNR contributes to the total response.

Now, at a certain wavelength the electric dipoles of all the individual GNRs are excited such that their local phase varies across the dielectric core sphere and a ring-type current is effectively induced. Such a state of collective excitation is what is conceptually shown in the left of Figure 10. The different

https://dx.doi.org/10.1021/acsanm.0c01346
ACS Appl. Nano Mater. 2020, 3, 6108−6117

phase relations of the induced electric dipoles in each individual GNR comes from the mutual coupling but also from the simple phase retardation of the incident field across the object that excites all the GNRs. That resonant excitation leads to a strong magnetic response. Please note, this finite spatial extent of the object and the phase variation of the incident field across the structure is necessary to obtain the magnetic response, which is indeed an effect due to spatial dispersion. Finally it is worth mentioning that the structure should not be too large as to prevent the notable excitation of higher order multipole moments. A possible intrinsic magnetic dipolar moment of the dielectric core sphere, as it is observed if the sphere would have been made from a material such as silicon, in the current scenario can be neglected in our structure, as the refractive index of the material from which the sphere is made is rather small. It does not allow sustaining a magnetic dipolar response in the wavelength region of interest and for the pertinent size. The structure of course supports, besides the magnetic dipolar mode, also other resonances that give rise to a particular multipolar composition of the scattering response. While higher order multipole moments are not very strongly excited because of the rather small size, an electric dipolar response can be excited resonantly, which can be seen in Figure 9 as well. The electric dipolar mode couples nicely to the far-field. Hence, its radiation losses are large and the resonance is quite broad. The type of excitation of all the individual dipoles in the GNR is shown in the right of Figure 10.

CONCLUSIONS

We have designed, fabricated, and characterized a novel kind of building block with a strong magnetic dipolar response that can serve as the basis for a future generation of self-assembled metamaterials fabricated with a bottom-up approach. Such materials could be applied for the preparation of perfect lenses or for cloaking. The structure consists of gold nanorods deposited on silica microspheres. Moreover, densely packed periodically arranged structures were achieved by using a blade coating deposition technique in which the silica microspheres were first deposited on a surface and afterward covered with GNRs with a dip-coating technique. Besides a structural analysis, the optical spectra of various samples were measured and compared to full-wave optical simulations. That helped to elucidate multiple effects that affect the spectral position of the resonances. Finally, based on simulations we could show that the response of the samples is linked to the resonant excitation of a magnetic dipolar response, something that does not exist for naturally occurring materials in the same spectral region.

The building blocks that we have introduced show an isotropic response and can be fabricated in large quantities. That means they constitute a solid base for an actual material that can be considered in the future for the realization of multiple applications relying on a dispersive magnetic response.

METHODS

Synthesis of Gold Nanorods. Gold nanorods (GNRs) of different aspect ratio were synthesized following a slightly modified seed-mediated growth method.[30] The seed-mediated growth method is a multistep process, in which GNRs are grown starting from small spherical seeds. Therefore, the first step consists in the preparation of the seed solution. In a 25 mL round-bottom flask, 5 mL of an aqueous solution of tetrachloroauric (III) acid ($HAuCl_4$, 0.5 mM) and 5 mL of an aqueous solution of cetyltrimethylammonium bromide (CTAB, 0.2 M) were stirred at 28 °C. Subsequently, 0.60 mL of an ice-cold aqueous solution of sodium borohydride ($NaBH_4$, 20 mM) was rapidly injected. The reaction was vigorously stirred for 4 min and then kept in an oil bath for at least another 15 min before being used. The second step involves the preparation of the growth solution. A 0.31 mL aliquot of an aqueous solution of silver nitrate ($AgNO_3$, 4 mM) was added to 25 mL of an aqueous solution of CTAB (0.2 M) in a 100 mL round-bottom flask at 28 °C. Then, 25 mL of an aqueous solution of $HAuCl_4$ (1 mM) was added, followed by 0.35 mL of an aqueous solution of ascorbic acid (AA, 78 mM). The third and last step involves the addition of the seeds into the growth solution. A few minutes after the growth solution was prepared, 80 μL of seed was injected and the reaction was kept overnight (12−15 h) under vigorous magnetic stirring at the constant temperature of 28 °C. This method allows obtaining a solution of GNRs with several aspect ratios by changing the content of silver ions.[39]

Functionalization of Silica Microspheres. To allow an electrostatic interaction between silica microspheres and GNRs for the fabrication of the core−shell clusters, the two components need to exhibit opposite surface charges. For this reason, the surface chemistry of the silica beads was modified. Silica microspheres (310 nm in diameter) were purchased from Bangs Laboratories, Inc (Indiana, USA). To impart a positive charge, 0.5 mL of the microspheres were added to 2 mL of a 5% (v/v) solution of *N*-[3-(trimethoxysilyl)-propyl]ethylenediamine (NTPE) in ethanol and stirred for 30 min. The solution was then centrifuged at 4000 rpm for 10 min in order to remove the excess of NTPE, which was then replaced by the same volume of ethanol.

Citrate Capping of Gold Nanorods. A conversion from CTAB-stabilized GNRs into citrate-stabilized GNRs was performed using the method of Mehtala et al.[33] with some modification. A 50 mL sample of CTAB-GNRs was first synthesized according to the seed-mediated growth method,[30] as described above. To prevent aggregation, the solution was diluted with milli-Q water to a final volume of 150 mL. The diluted solution of GNRs was divided into six centrifuge tubes (25 mL in each tube) that were then subjected to three cycles of centrifugation at 6500 rpm for 60 min in milli-Q water. The third cycle ended with the redispersion of all GNRs in 100 mL of sodium polystyrenesulfonate (Na-PSS, 0.15 wt %) and the solution was then allowed to sit for at least 1 h. After this waiting time, the suspension was subjected to an additional centrifugation cycle at 7500 rpm for 30 min. Then, the supernatant was removed and the GNRs redispersed again in three centrifuge tubes, each filled with 30 mL of Na-PSS (0.15 wt %). The PSS-GNRs were then subjected to two more centrifugation cycles at 7500 rpm for 30 min, with redispersion in 30 mL of aqueous solution of sodium citrate (5 mM) for the exchange with PSS. Between these last two cycles, the GNRs suspension was allowed to sit for at least 12 h. The resulting citrate-capped GNR dispersion was stable at room temperature for at least 1 year.

Coating Silica Microspheres with Gold Nanorods (Core−Shell Clusters in Solution). Core−shell clusters were produced following the method introduced by Mühlig et al.[9] A 10 μL drop of the functionalized silica core sphere solution was injected into 40 mL of citrate-capped GNRs solution under vigorous stirring at room temperature. To achieve dense GNR coverage on the silica microspheres surface, the concentration of core spheres has to be much lower relative to the concentration of the GNRs.

Gold Nanorods Deposition on Silica Microspheres Monolayer Prepared via Blade Coating (Core−Shell Clusters Array). For this experiment, the thermostat connected to the blade coater was set to 32 °C. Glass microscope slides, used as both substrates and blades, were cleaned with Piranha solution (3:1 mixture of sulfuric acid to hydrogen peroxide 30%) for at least 30 min before use. To warm up, the substrate was fixed on the hot aluminum plate at least 20 min before starting the deposition. Aqueous dispersions of monodispersed silica microspheres (diameter 304 nm, coefficient of variation 2.3%) were purchased from microParticles GmbH. A high degree of monodispersity is required to achieve a close-packed monolayer. The microspheres concentration was adjusted to a value

https://dx.doi.org/10.1021/acsanm.0c01346
ACS Appl. Nano Mater. 2020, 3, 6108−6117

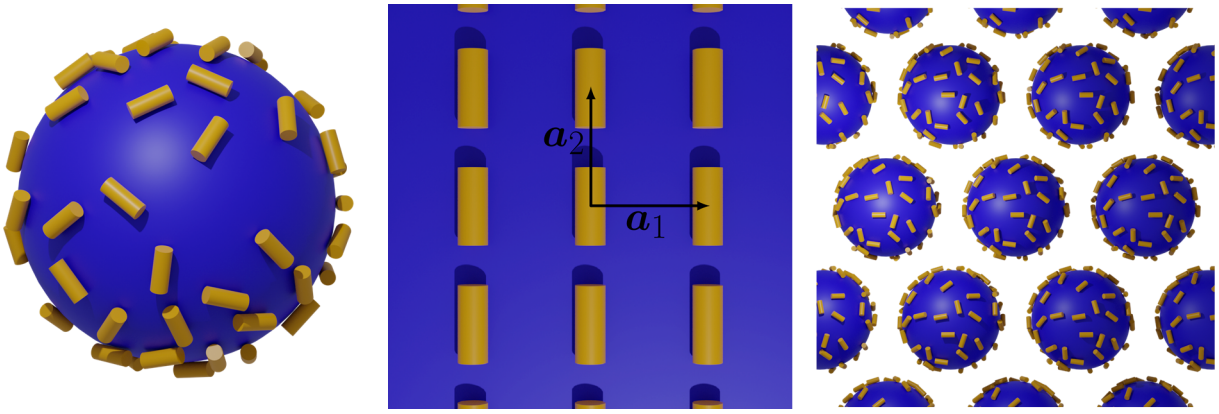

Figure 11. Arrangement of the GNRs on the sphere and on the substrate. The length of the lattice vectors is averaged over the range between 40 and 83.3 nm while keeping the density of GNRs constant.

of 2% of solid content by dilution with milli-Q water. A small volume of solution (approximately 50 μL) was injected with a syringe between the substrate and the blade fixed at the acute angle of 50° above the substrate at a distance of approximately 0.04 mm. The substrate was moved at a speed of 0.02 mm/sec. The experimental setup was enclosed in a plexiglass chamber together with moisture-sensitive silica beads to control and to keep the ambient humidity constant at a value of 37%. The temperature of the substrate was maintained at 32° for the entire duration of the deposition.

The as prepared monolayer was then heated in a furnace at 500 °C for 3 h to covalently bind the silica microspheres to the surface of the glass substrate. Afterward, the sample was immersed in H_2O_2 for 30 min to create hydroxyl groups on the surface and to obtain a better adhesion of the coating nanoparticles solution. To adsorb the GNRs onto the silica microspheres monolayer, it was then necessary to alter the surface chemistry of the deposited monolayer to induce an affinity between both constituents. The sample was thus immersed in a 5% (v/v) solution of *N*-[3-(trimethoxysilyl)propyl]ethylenediamine in ethanol for 30 min and then rinsed with milli-Q water. Excess water was removed using a stream of nitrogen followed by drying in a furnace at 120 °C for 30 min to ensure good silanization. After functionalization, the GNRs could be deposited via dip coating onto the monolayer of silica microspheres. After the sample was allowed to cool spontaneously, it was dipped in a solution of PSS in water (5 mg/mL) and 1 M sodium chloride (NaCl) for 5 min. After being rinsed with milli Q-water and dried, the sample was immersed in a solution of GNRs capped with CTAB for 2 h.

Characterization Techniques and Simulations. *Microscopy Characterization.* TEM imaging was carried out on a Tecnai G2 Sphera transmission electron microscope from FEI, operating at an accelerating voltage of 120 kV. The samples were deposited on carbon-coated copper TEM grids (3.05 mm in diameter, with different mesh sizes). SEM was performed on a JEOL JSM-7600F microscope.

Surface Characterization. ζ-Potential measurements were performed at 25 °C using the Zetasizer Nano ZS from Malvern. The samples for measurements were used as prepared, without dilution. Five runs and ten sub-runs per sample were performed to ensure measurement repeatability.

Optical Characterization. UV−vis spectra were measured on a Cary Varian 50 Bio UV−visible spectrophotometer and on a Jasco V-670 UV−vis/NIR spectrophotometer.

Simulations. The simulations of the GNRs in the different configurations, that is, in solution, deposited on silica spheres, and deposited on planar glass substrates, were done in two steps. The initial step in each configuration is the computation of the T-matrix of the gold[40] nanorods, which was done numerically[41,42] using the commercial finite element solver JCMsuite.[43] The permittivity of gold was taken from Johnson and Christy.[33] For the computation we exploited the cylindrical symmetry of the nanorods to use a two-dimensional domain, and took perfectly matched layers to get a transparent boundary. The maximum expansion for the multipoles was set to $l_{max} = 4$, which provides a sufficient accuracy.

Since the T-matrix contains the full scattering information on an object, the extinction cross section of a single nanorod can be computed directly from its coefficients.[44] The extinction cross section averaged over all angles of a single nanorod provides the extinction of many such nanorods in solution by choosing a respective embedding medium characterized by a refractive index of $n = 1.333$. The angular averaging takes into account all possible orientations of the nanorods. The length of the nanorods was chosen to be 38 nm and its diameter was 15 nm, in agreement with a nominal size of an average nanorod as observed in SEM images. The GNR can be considered as the typical size for the GNRs expected to be found in the solution. In the experiment, with solutions containing GNRs with variations in length and radius, a broadened line width is expected in comparison to the computed line width of a solution containing nanorods of a single specific geometry.

To obtain the extinction of GNRs covering the silica microsphere, the T-matrix of this composite object is computed. This is done by the analytical coupling of the T-matrices of the GNRs with the T-matrix of the silica sphere.[45] The refractive index is taken to be $n = 1.5$. In contrast to the GNRs, the T-matrix of a sphere can be computed analytically,[46] due to its rotational symmetry. A matching multipole order of $l_{max} = 4$ is chosen for it. The sphere and the GNRs are taken to be in air. Thus, the computation of the GNR's T-matrices is repeated with an embedding of a refractive index of $n = 1$. For the calculation of the electromagnetic interaction, the positions of the GNRs on the sphere are chosen at random positions on its surface with the requirement that the GNRs do not touch each other. In total, 60 GNRs are distributed on the sphere to represent the expected conditions in the experiment. The actual arrangement in shown in Figure 11. From the entire core−shell particle, the extinction cross section can again be obtained directly as in the case of the GNRs in solution. Also, the extinction can be calculated for a periodic arrangement of such structures.[47]

To obtain the extinction of the random arrangement of the GNRs on a glass substrate, a straightforward computation as in the other two cases is not possible due to the sheer size of the system. Thus, a different approach is chosen, where the GNRs are distributed on a two-dimensional periodic lattice. The periodic geometry allows employing an efficient algorithm to sum up the multiple scattering interaction of all GNRs and the inclusion of the substrate.[48] A solvent is no longer present. The conditions found in the experiment are taken into account as follows. The density of the particles was taken to be 300 GNRs per μm^2, which is estimated from SEM images. Since in a random distribution various coupling scenarios occur, the extinction calculation is averaged over multiple rectangular lattices with different aspect ratios of the unit cell. The unit cells go from 40 nm by 83.3 nm to the opposite, 83.3 nm by 40 nm. The minimal

https://dx.doi.org/10.1021/acsanm.0c01346
ACS Appl. Nano Mater. 2020, 3, 6108−6117

distance of 40 nm is chosen such that the GNRs with a length of 38 nm nearly touch. Thus, coupling scenarios with strong interaction of the GNRs, for example if they are closely parallel or with touching tips, are taken into account. For the extinction calculation, the transmittance, reflection, and absorption are calculated for a plane wave with unit power as illumination. The plane wave is taken to impinge on the lattice under normal incidence. The response has been polarization averaged to account for the random orientation of the GNRs on the glass substrate.

Finally, for the core−shell particles on the array, we use the same computation method as for the GNRs on the substrate. The method to obtain their T-matrices is described above. According to the SEM images of the blade-coated structures in Figure 6, they are placed on a hexagonal lattice with the lattice constant set to 400 nm. The array structure used in the simulation is shown in Figure 11. Below the array the glass substrate is placed like in the case of the GNR monolayer.

AUTHOR INFORMATION

Corresponding Authors

Rossella Grillo − *Department of Physical Chemistry, University of Geneva, Geneva 4 1211, Switzerland*; Email: rossella.grillo@unirc.it

Thomas Bürgi − *Department of Physical Chemistry, University of Geneva, Geneva 4 1211, Switzerland*; orcid.org/0000-0003-0906-082X; Email: thomas.buergi@unige.ch

Authors

Dominik Beutel − *Institute of Theoretical Solid State Physics, Karlsruhe Institute of Technology, Karlsruhe 76131, Germany*

Ugo Cataldi − *Department of Physical Chemistry, University of Geneva, Geneva 4 1211, Switzerland*

Carsten Rockstuhl − *Institute of Theoretical Solid State Physics, Karlsruhe Institute of Technology, Karlsruhe 76131, Germany; Institute of Nanotechnology, Karlsruhe Institute of Technology, Eggenstein-Leopoldshafen 76344, Germany*

Complete contact information is available at: https://pubs.acs.org/10.1021/acsanm.0c01346

Notes

The authors declare no competing financial interest.

ACKNOWLEDGMENTS

The authors thank University of Geneva and the Swiss National Science Foundation (Grant No. 200021L_156184) for supporting this work. We also acknowledge support by the Deutsche Forschungsgemeinschaft (DFG, German Research Foundation) under Germany's Excellence Strategy—EXC 2082/1-390761711 and under the project RO 3640/4-1. D.B. acknowledges support from the Carl Zeiss Foundation via the CZF-Focus@HEiKA program. The authors are grateful to the company JCMwave for their free provision of the FEM Maxwell solver JCMsuite with which the T-matrices of the nonspherical structures discussed in this work were calculated.

ABBREVIATIONS

LSPP = localized surface plasmon polariton
LSPR = localized surface plasmon resonance
GNRs = gold nanorods
CTAB = cetyltrimethylammonium bromide
NTPE = *N*-[3-(trimethoxysilyl)propyl]ethylenediamine
PSS = polystyrenesulfonate
TEM = transmission electron microscopy
SEM = scanning electron microscopy
AR = aspect ratio

REFERENCES

(1) Mühlig, S.; Farhat, M.; Rockstuhl, C.; Lederer, F. Cloaking Dielectric Spherical Objects by a Shell of Metallic Nanoparticles. *Phys. Rev. B: Condens. Matter Mater. Phys.* **2011**, *83* (19), 195116.

(2) Pastoriza-Santos, I.; Gomez, D.; Pe, J.; Liz-Marzan, L. M.; Mulvaney, P. Optical Properties of Metal Nanoparticle Coated Silica Spheres: A Simple Effective Medium Approach. *Phys. Chem. Chem. Phys.* **2004**, *6*, 5056−5060.

(3) Lu, Z.; Goebl, J.; Ge, J.; Yin, Y. Self-Assembly and Tunable Plasmonic Property of Gold Nanoparticles on Mercapto-Silica Microspheres. *J. Mater. Chem.* **2009**, *19* (26), 4597−4602.

(4) Le Beulze, A.; Gomez-Graña, S.; Gehan, H.; Mornet, S.; Ravaine, S.; Correa-Duarte, M.; Guerrini, L.; Alvarez-Puebla, R. A.; Duguet, E.; Pertreux, E.; Crut, A.; Maioli, P.; Vallée, F.; Del Fatti, N.; Ersen, O.; Treguer-Delapierre, M. Robust Raspberry-like Metallo-Dielectric Nanoclusters of Critical Sizes as SERS Substrates. *Nanoscale* **2017**, *9* (17), 5725−5736.

(5) Simovski, C. R.; Tretyakov, S. A. Model of Isotropic Resonant Magnetism in the Visible Range Based on Core-Shell Clusters. *Phys. Rev. B: Condens. Matter Mater. Phys.* **2009**, *79* (4), 045111.

(6) Barois, P.; Ponsinet, V.; Baron, A.; Richetti, P. Bottom-up Production of Meta-Atoms for Optical Magnetism in Visible and NIR Light. *J. Phys.: Conf. Ser.* **2018**, *963*, 012007.

(7) Many, V.; Dézert, R.; Duguet, E.; Baron, A.; Jangid, V.; Ponsinet, V.; Ravaine, S.; Richetti, P.; Barois, P.; Tréguer-Delapierre, M. High Optical Magnetism of Dodecahedral Plasmonic Meta-Atoms. *Nanophotonics* **2018**, *8*, 549−558.

(8) Gomez-Graña, S.; Le Beulze, A.; Treguer-Delapierre, M.; Mornet, S.; Duguet, E.; Grana, E.; Cloutet, E.; Hadziioannou, G.; Leng, J.; Salmon, J. B.; Kravets, V. G.; Grigorenko, A. N.; Peyyety, N. A.; Ponsinet, V.; Richetti, P.; Baron, A.; Torrent, D.; Barois, P. Hierarchical Self-Assembly of a Bulk Metamaterial Enables Isotropic Magnetic Permeability at Optical Frequencies. *Mater. Horiz.* **2016**, *3* (6), 596−601.

(9) Mühlig, S.; Cunningham, A.; Scheeler, S.; Pacholski, C.; Bürgi, T.; Rockstuhl, C.; Lederer, F. Self-Assembled Plasmonic Core-Shell Clusters with an Isotropic Magnetic Dipole Response in the Visible Range. *ACS Nano* **2011**, *5* (8), 6586−6592.

(10) Ponsinet, V.; Barois, P.; Gali, S. M.; Richetti, P.; Salmon, J. B.; Vallecchi, A.; Albani, M.; Le Beulze, A.; Gomez-Grana, S.; Duguet, E.; Mornet, S.; Treguer-Delapierre, M. Resonant Isotropic Optical Magnetism of Plasmonic Nanoclusters in Visible Light. *Phys. Rev. B: Condens. Matter Mater. Phys.* **2015**, *92* (22), 2−6.

(11) Alù, A.; Salandrino, A.; Engheta, N. Negative Effective Permeability and Left-Handed Materials at Optical Frequencies. *Opt. Express* **2006**, *14* (4), 1557−1567.

(12) Pendry, J. B. Negative Refraction Makes a Perfect Lens. *Phys. Rev. Lett.* **2000**, *85* (18), 3966−3967.

(13) Leonhardt, U.; G. Philbin, T. Transformation Optics and the Geometry of Light. In *Progress in Optics*; Emil, W., Ed.; Elsevier, 2009.

(14) Smith, D. R.; Padilla, W. J.; Vier, D. C.; Nemat-Nasser, S. C.; Schultz, S. Composite Medium with Simultaneously Negative Permeability and Permittivity. *Phys. Rev. Lett.* **2000**, *84* (18), 4184−4187.

(15) Sabah, C. Electric and Magnetic Excitations in Anisotropic Broadside-Coupled Triangular-Split-Ring Resonators. *Appl. Phys. A: Mater. Sci. Process.* **2012**, *108* (2), 457−463.

(16) Zhao, Q.; Zhou, J.; Zhang, F.; Lippens, D. Mie Resonance-Based Dielectric Metamaterials. *Mater. Today* **2009**, *12* (12), 60−69.

(17) Yannopapas, V.; Vitanov, N. V. Photoexcitation-Induced Magnetism in Arrays of Semiconductor Nanoparticles with a Strong Excitonic Oscillator Strength. *Phys. Rev. B: Condens. Matter Mater. Phys.* **2006**, *74*, 193304.

(18) García-Etxarri, A.; Gómez-Medina, R.; Froufe-Pérez, L. S.; López, C.; Chantada, L.; Scheffold, F.; Aizpurua, J.; Nieto-Vesperinas, M.; Sáenz, J. J. Strong Magnetic Response of Submicron Silicon Particles in the Infrared. *Opt. Express* **2011**, *19* (6), 4815−4826.

https://dx.doi.org/10.1021/acsanm.0c01346
ACS Appl. Nano Mater. 2020, 3, 6108−6117

(19) Kuznetsov, A. I.; Miroshnichenko, A. E.; Fu, Y. H.; Zhang, J.; Lukyanchukl, B. Magnetic Light. *Sci. Rep.* **2012**, *2*, 492.
(20) Zeng, J.; Darvishzadeh-Varcheie, M.; Albooyeh, M.; Rajaei, M.; Kamandi, M.; Veysi, M.; Potma, E. O.; Capolino, F.; Wickramasinghe, H. K. Exclusive Magnetic Excitation Enabled by Structured Light Illumination in a Nanoscale Mie Resonator. *ACS Nano* **2018**, *12* (12), 12159−12168.
(21) Dietrich, K.; Zilk, M.; Steglich, M.; Siefke, T.; Hübner, U.; Pertsch, T.; Rockstuhl, C.; Tünnermann, A.; Kley, E. B. Merging Top-Down and Bottom-Up Approaches to Fabricate Artificial Photonic Nanomaterials with a Deterministic Electric and Magnetic Response. *Adv. Funct. Mater.* **2020**, *30* (3), 1905722.
(22) Manna, U.; Lee, J. H.; Deng, T. S.; Parker, J.; Shepherd, N.; Weizmann, Y.; Scherer, N. F. Selective Induction of Optical Magnetism. *Nano Lett.* **2017**, *17*, 7196−7206.
(23) Schurig, D.; Mock, J. J.; Justice, B. J.; Cummer, S. A.; Pendry, J. B.; Starr, A. F.; Smith, D. R. Metamaterial Electromagnetic Cloak at Microwave Frequencies. *Science (Washington, DC, U. S.)* **2006**, *314* (5801), 977−980.
(24) Waterman, P. C. Matrix Formulation of Electromagnetic Scattering. *Proc. IEEE* **1965**, *53* (8), 805−812.
(25) Salgueiriño-Maceira, V.; Caruso, F.; Liz-Marzán, L. M. Coated Colloids with Tailored Optical Properties. *J. Phys. Chem. B* **2003**, *107* (40), 10990−10994.
(26) Ashayer, R.; Mannan, S. H.; Sajjadi, S. Synthesis and Characterization of Gold Nanoshells Using Poly(Diallyldimethyl Ammonium Chloride). *Colloids Surf., A* **2008**, *329* (3), 134−141.
(27) Sheikholeslami, S. N.; Alaeian, H.; Koh, A. L.; Dionne, J. A. A Metafluid Exhibiting Strong Optical Magnetism. *Nano Lett.* **2013**, *13* (9), 4137−4141.
(28) Sadtler, B.; Wei, A. Spherical Ensembles of Gold Nanoparticles on Silica: Electrostatic and Size Effects. *Chem. Commun.* **2002**, *2* (15), 1604−1605.
(29) Malaquin, L.; Kraus, T.; Schmid, H.; Delamarche, E.; Wolf, H. Controlled Particle Placement through Convective and Capillary Assembly. *Langmuir* **2007**, *23* (23), 11513−11521.
(30) Nikoobakht, B.; El-Sayed, M. A. Preparation and Growth Mechanism of Gold Nanorods (NRs) Using Seed-Mediated Growth Method. *Chem. Mater.* **2003**, *15*, 1957−1962.
(31) Toderas, F.; Iosin, M.; Astilean, S. Luminescence Properties of Gold Nanorods. *Nucl. Instrum. Methods Phys. Res., Sect. B* **2009**, *267* (2), 400−402.
(32) Link, S.; Mohamed, M. B.; El-Sayed, M. A. Simulation of the Optical Absorption Spectra of Gold Nanorods as a Function of Their Aspect Ratio and the Effect of the Medium Dielectric Constant. *J. Phys. Chem. B* **2002**, *103* (16), 3073−3077.
(33) Mehtala, J. G.; Zemlyanov, D. Y.; Max, J. P.; Kadasala, N.; Zhao, S.; Wei, A. Citrate-Stabilized Gold Nanorods. *Langmuir* **2014**, *30* (46), 13727−13730.
(34) Alkilany, A. M.; Nagaria, P. K.; Hexel, C. R.; Shaw, T. J.; Murphy, C. J.; Wyatt, M. D. Cellular Uptake and Cytotoxicity of Gold Nanorods: Molecular Origin of Cytotoxicity and Surface Effects. *Small* **2009**, *5* (6), 701−708.
(35) Scarabelli, L.; Sánchez-Iglesias, A.; Pérez-Juste, J.; Liz-Marzán, L. M. A "Tips and Tricks" Practical Guide to the Synthesis of Gold Nanorods. *J. Phys. Chem. Lett.* **2015**, *6* (21), 4270−4279.
(36) Funston, A. M.; Novo, C.; Davis, T. J.; Mulvaney, P. Plasmon Coupling of Gold Nanorods at Short Distances and in Different Geometries. *Nano Lett.* **2009**, *9* (4), 1651−1658.
(37) Dincau, B. M.; Bazant, M. Z.; Dressaire, E.; Sauret, A. Capillary Sorting of Particles by Dip Coating. *Phys. Rev. Appl.* **2019**, *12* (1), 011001.
(38) Alaee, R.; Rockstuhl, C.; Fernandez-Corbaton, I. Exact Multipolar Decompositions with Applications in Nanophotonics. *Adv. Opt. Mater.* **2019**, *7* (1), 1800783.
(39) Ward, C. J.; Tronndorf, R.; Eustes, A. S.; Auad, M. L.; Davis, E. W. Seed-Mediated Growth of Gold Nanorods: Limits of Length to Diameter Ratio Control. *J. Nanomater.* **2014**, *2014*, 765618.
(40) Johnson, P. B.; Christy, R. W. Optical Constant of the Nobel Metals. *Phys. Rev. B* **1972**, *6* (12), 4370−4379.
(41) Demésy, G.; Auger, J.-C.; Stout, B. Scattering Matrix of Arbitrarily Shaped Objects: Combining Finite Elements and Vector Partial Waves. *J. Opt. Soc. Am. A* **2018**, *35* (8), 1401.
(42) Fruhnert, M.; Fernandez-Corbaton, I.; Yannopapas, V.; Rockstuhl, C. Computing the T-Matrix of a Scattering Object with Multiple Plane Wave Illuminations. *Beilstein J. Nanotechnol.* **2017**, *8* (1), 614−626.
(43) Burger, S.; Zschiedrich, L.; Pomplun, J.; Schmidt, F. JCMsuite: An Adaptive FEM Solver for Precise Simulations in Nano-Optics. *Integrated Photonics and Nanophotonics Research and Applications; Optical Society of America* **2008**, No. ITuE4.
(44) Mishchenko, M. I.; Travis, L. D.; Mackowski, D. W. T-Matrix Computations of Light Scattering by Nonspherical Particles: A Review. *J. Quant. Spectrosc. Radiat. Transfer* **1996**, *55* (5), 535−575.
(45) Tsang, L.; Kong, J. A.; Shin, R. T. *Theory of Microwave Remote Sensing*; Wiley Series in Remote Sensing and Image Processing (Book 2); Wiley: 1985.
(46) Bohren, C. F.; Huffman, D. R. *Absorption and Scattering of Light by Small Particles*; Wiley: 1998.
(47) Stefanou, N.; Yannopapas, V.; Modinos, A. MULTEM 2: A New Version of the Program for Transmission and Band-Structure Calculations of Photonic Crystals. *Comput. Phys. Commun.* **2000**, *132* (1−2), 189−196.
(48) Stefanou, N.; Yannopapas, V.; Modinos, A. Heterostructures of Photonic Crystals: Frequency Bands and Transmission Coefficients. *Comput. Phys. Commun.* **1998**, *113*, 49−77.

https://dx.doi.org/10.1021/acsanm.0c01346
ACS Appl. Nano Mater. 2020, 3, 6108−6117